An adaptive harmonic balance method for predicting the nonlinear dynamic responses of mechanical systems—Application to bolted structures

V. Jaumouillé [a,b], J.-J. Sinou [a,*], B. Petitjean [b]

[a] Laboratoire de Tribologie et Dynamique des Systèmes UMR-CNRS 5513, Ecole Centrale de Lyon, 36 avenue Guy de Collongue, 69134 Ecully Cedex, France
[b] EADS Innovation Works, 12 rue Pasteur, 92150 Suresnes, France

ARTICLE INFO

ABSTRACT

Aeronautical structures are commonly assembled with bolted joints in which friction phenomena, in combination with slapping in the joint, provide damping on the dynamic behavior. Some models, mostly nonlinear, have consequently been developed and the harmonic balance method (HBM) is adapted to compute nonlinear response functions in the frequency domain. The basic idea is to develop the response as Fourier series and to solve equations linking Fourier coefficients. One specific HBM feature is that response accuracy improves as the number of harmonics increases, at the expense of larger computational time. Thus this paper presents an original adaptive HBM which adjusts the number of retained harmonics for a given precision and for each frequency value. The new proposed algorithm is based on the observation of the relative variation of an approximate strain energy for two consecutive numbers of harmonics. The developed criterion takes the advantage of being calculated from Fourier coefficients avoiding time integration and is also expressed in a condensation case. However, the convergence of the strain energy has to be smooth on tested harmonics and this constitutes a limitation of the method. Condensation and continuation methods are used to accelerate calculation. An application case is selected to illustrate the efficiency of the method and is composed of an asymmetrical two cantilever beam system linked by a bolted joint represented by a nonlinear LuGre model. The practice of adaptive HBM shows that, for a given value of the criterion, the number of harmonics increases on resonances indicating that nonlinear effects are predominant. For each frequency value, convergence of approximate strain energy is observed. Emergence of third and fifth harmonics is noticed near resonances both on vibratory responses and on approximate strain energy. Parametric studies are carried out by varying the excitation force amplitude and the threshold value of the adaptive algorithm. Maximal amplitudes of vibration and frequency response functions are plotted for three different points of the structure. Nonlinear effects become more predominant for higher force amplitudes and consequently the number of retained harmonics is increased.

© 2010 Elsevier Ltd. All rights reserved.

1. Introduction

The dynamics of mechanical structures is strongly influenced by the presence of riveted or bolted joints in the structure. Indeed structural joints generate energy dissipation through the complex relative motion between two contacting surfaces,

---

* Corresponding author. Tel.: +33 4 72 18 64 66.
E-mail address: jean-jacques.sinou@ec-lyon.fr (J.-J. Sinou).

commonly referred as frictional slip. Additionally for higher level of excitation, slapping may be encountered. Frictional slip may be analyzed by considering an interface behavior divided in two cases: micro-slip where part of the interface is slipping; and macro-slip where all the interface slips. Then the frictional energy dissipation observed in the slip zone is responsible for the vibration damping attributed to joints [1]. Gaul et al. [2] showed that this damping may be larger than material damping and Beards [3] mentioned that up to 90 percent of the total system damping might be provided by the joints. Thorough reviews about damping in joints may be found in the works of Ungar [4], Gaul et al. [2] and more recently Ibrahim et al. [5].

A better prediction of this damping effect is now an important objective for many aeronautical companies and various complex industrial structures incorporating bolted joints have been investigated [6–9]. Crocombe et al. [7] established a relationship between energy dissipated in a joint and the transverse excitation force using a 3D FE model of a bolted joint and then used this relationship in conjunction with the simulation of a FE model of a satellite to estimate the energy dissipated in the joints. In the work of Caignot [9], a micro scale model of bolted joints quantifies in a first step the joint dissipation and an equivalent modal damping is deduced in a second step to perform dynamic analysis of the whole studied structure.

These approaches perform a complex contact analysis giving an insight into the distribution and amount of friction on the interfaces but neglect nonlinear effects in the global dynamic behavior of the assembled bolted structure. They need detailed models, often impractical for dynamic analyses of large structures. Hence constitutive models which use a number of degrees of freedom adapted to structural dynamics may be a suitable and computationally efficient alternative. These models can be divided into lumped models and thin layer element theories [10]. In lumped models, the effect of joint is considered to be concentrated at a single point and the joint model has no dimension. Several models have been proposed: the Valanis model [11], the elasto-slip model [2], the LuGre model [2], the Iwan model [1], the Bouc–Wen model [12], models with Jenkins elements [12] and models integrating a cubic stiffness [13]. The second category, based on thin layer elements, is represented as an element with physical dimensions and specific force–displacement relation. Ahmadian et al. [10] developed a generic joint element based on a thin layer element approach and Song et al. [14] developed an adjusted Iwan beam element incorporating an Iwan model to simulate the dynamics of beam structures.

Most of these models are nonlinear and require specific methods to compute nonlinear frequency response functions. In order to compute responses to forced excitation, one of the first methods is time integration. Oldfield et al. [12] applied time integration on a bolted structure to simulate hysteresis loops using a Jenkins element model and a Bouc–Wen model. Other applications on a two beam system were encountered in the works of Gaul et al. [11] and Miller et al. [15]. Time integration may be inefficient on lightly damped structures because the transient response may take hundreds of forcing periods at the expense of calculation time and disc storage size. Other alternatives like perturbation methods and the Krylov and Bogoliubov method remain limited to a few degrees of freedom. Heller et al. [16] applied the Krylov–Bogoliubov method on a nonlinear system in order to determine equivalent modal parameters and not to compute periodic responses.

In the frequency domain, the harmonic balance method (HBM) is able to compute periodic responses of nonlinear systems. The basics are to develop the unknown response as a truncated Fourier series and to solve equations linking Fourier coefficients. First mechanical applications can be encountered in the works of Pierre et al. [17] on a single degree of freedom dry friction damped system and Ferri et al. [18] on a beam incorporating dry friction. Then a further development of the HBM, named alternating frequency time domain method [19], numerically evaluates the Fourier transform of local nonlinearities of the model and does not require to analytically describe nonlinear terms. More recently, other approaches have been proposed, notably the constrained harmonic balance method [20] which computes solutions for periodic autonomous systems. For dynamic analyses of bolted joints, Gaul et al. [2] used harmonic balance method for the calculation of an equivalent stiffness and viscous damping in an elasto-slip model. Ren et al. [21] proposed a general technique for identifying the dynamic properties of nonlinear joints using dynamic test data and used multi-harmonic balance method to identify parameters for a friction joint. These two developments compute hysteresis loops and not periodic responses. The work of Ahmadian et al. [10] developed a nonlinear generic element formulation for bolted joints and used a cubic nonlinear stiffness to represent softening nonlinear effects. Then frequency response curves of the system are calculated with the HBM allowing to include these curves in a minimization procedure in order to identify parameters of the joint. Only prime harmonics were considered due to experimental considerations.

One specific HBM feature is that response accuracy improves as the number of harmonics in the truncated Fourier series increases, at the expense of larger computational time. Therefore only harmonics which lead to a significant contribution on dynamic response must be taken into account for a given precision, and their number can strongly vary on a frequency interval.

This key point has been highlighted for bolted joint dynamics by Ouyang et al. [22] who studied an experimental two beam bolted system excited at resonance. By increasing importance of friction in the joints (through an increase of the excitation amplitude), measured hysteresis loops became distorted and superharmonics appeared in the frequency spectra of the responses, showing the importance of considering higher order terms in the Fourier development of the response. Only odd harmonics were present suggesting the possibility to use a cubic stiffness in the bolted joint model [10,13] and to only consider odd harmonics in the harmonic balance method, usual practice for dry friction system [17].

Even though, up to now, no theoretical tool can determine which harmonics are predominant for a nonlinear system. The present study pursues this investigation by developing a criterion allowing to limit the number of retained harmonics.

An approximate strain energy with Fourier coefficients is calculated and its saturation is monitored. This new criterion, based on Fourier coefficients, does not require time integration and may be easily estimated. In order to illustrate the efficiency of the method on a nonlinear mechanical system, an asymmetrical two cantilever beam system linked by a bolted joint is modelled as application case. The joint model was inspired by the adjusted Iwan beam element (AIBE) developed by Song [14]. However, a LuGre model was preferred to an Iwan model present in the work of Song for implementation simplicity. Moreover, formulation of HBM has consequently been adapted to integrate LuGre model internal variables. Analysis of frequency response functions and detailed monitoring of criterion evolution help to assess the validity of this approach. In order to accelerate calculation, a condensation procedure on nonlinear degrees of freedom is performed by reformulating the HBM equations. Furthermore, criterion has been expressed in this case and compared with case without condensation.

This paper is divided into three main sections. The first one deals with the HBM formulation, details condensation and criterion expression. Secondly, the studied system is presented and HBM adaptation to LuGre model is detailed. Finally, result analyses highlight the effect of the harmonic selection process on frequency response functions and on the number of retained harmonics, and a parametric study on the influence of the excitation force is discussed.

2. HBM formulation

2.1. General formulation

We consider a discrete mechanical system with $nddl$ degrees of freedoms (dofs) described with its $nddl \times nddl$ mass matrix $\mathbf{M}$, stiffness matrix $\mathbf{K}$ and damping matrix $\mathbf{D}$). An external periodic force $F_L(\Omega,t)$ is applied to the system with an angular frequency Ω. System nonlinearities are considered as a nonlinear force $F_{NL}(X,\dot{X},\Omega,t)$ which depends on degrees of freedom displacements X, velocities $\dot{X}$, angular frequency Ω and time t. The global force $F(X,\dot{X},\Omega,t)$ applied on the system may be divided in two parts, the linear external force $F_L(\Omega,t)$ and the nonlinear force $F_{NL}(X,\dot{X},\Omega,t)$. The governing equation of motion may be written as

$$\mathbf{M}\ddot{X} + \mathbf{D}\dot{X} + \mathbf{K}X = F(X,\dot{X},\Omega,t) = F_L(\Omega,t) + F_{NL}(X,\dot{X},\Omega,t) \tag{1}$$

First, we assume a periodic response $X(t)$, which allows to develop the solution as a Fourier series. This development is theoretically infinite so a truncation in the following form is needed:

$$X(t) = B_0 + \sum_{k=1}^{m} \left(A_k \sin\left(\frac{k}{v}\Omega t\right) + B_k \cos\left(\frac{k}{v}\Omega t\right) \right)$$

$$X(t) = \left[\mathbf{I} \quad \sin\left(\frac{\Omega}{v}t\right)\mathbf{I} \quad \cos\left(\frac{\Omega}{v}t\right)\mathbf{I} \quad \ldots \quad \sin\left(\frac{k}{v}\Omega t\right)\mathbf{I} \quad \cos\left(\frac{k}{v}\Omega t\right)\mathbf{I} \quad \ldots \right][B_0\ A_1\ B_1\ \ldots\ A_k\ B_k\ \ldots]^{\mathrm{T}}$$

$$X(t) = \mathbf{T}(t)Z \tag{2}$$

where $\mathbf{I}$ is the $nddl \times nddl$ identity matrix, $Z = [B_0\ A_1\ B_1\ \ldots\ A_k\ B_k\ \ldots]^{\mathrm{T}}$ is the $(2m+1)nddl \times 1$ vector containing Fourier coefficients, m is the number of harmonics retained for the truncation, v is an integer used to represent possible subharmonics, and $\mathbf{T}(t) = [\mathbf{I}\ \sin(\frac{\Omega}{v}t)\mathbf{I}\ \cos(\frac{\Omega}{v}t)\mathbf{I}\ \ldots\ \sin(\frac{k}{v}\Omega t)\mathbf{I}\ \cos(\frac{k}{v}\Omega t)\mathbf{I}\ \ldots]$ is the $nddl \times (2m+1)nddl$ matrix containing trigonometric functions.

The same work is then accomplished for the global force F:

$$F(X,\dot{X},\Omega,t) = C_0 + \sum_{k=1}^{m} \left(S_k \sin\left(\frac{k}{v}\Omega t\right) + C_k \cos\left(\frac{k}{v}\Omega t\right) \right)$$

$$F(X,\dot{X},\Omega,t) = \mathbf{T}(t)[C_0\ S_1\ C_1\ \ldots\ S_k\ C_k\ \ldots]^{\mathrm{T}}$$

$$F(X,\dot{X},\Omega,t) = \mathbf{T}(t)b \tag{3}$$

In order to compute velocities and accelerations, we define a frequential derivative operator:

$$\boldsymbol{\nabla} = \mathrm{diag}(\mathbf{0}_{nddl \times nddl}, \boldsymbol{\nabla}_1, \ldots, \boldsymbol{\nabla}_m) \quad \text{with} \quad \boldsymbol{\nabla}_k = \frac{k}{v}\Omega \begin{bmatrix} \mathbf{0} & -\mathbf{I} \\ \mathbf{I} & \mathbf{0} \end{bmatrix} \tag{4}$$

Thus we may write:

$$\dot{X}(t) = \mathbf{T}(t)\boldsymbol{\nabla}Z$$

$$\ddot{X}(t) = \mathbf{T}(t)\boldsymbol{\nabla}^2 Z \tag{5}$$

By replacing Eqs. (2) and (5) into Eq. (1), one obtains:

$$\mathbf{M}\mathbf{T}(t)\boldsymbol{\nabla}^2 Z + \mathbf{D}\mathbf{T}(t)\boldsymbol{\nabla}Z + \mathbf{K}\mathbf{T}(t)Z = \mathbf{T}(t)b \tag{6}$$

Considering that for a $nddl \times nddl$ matrix $\mathbf{W}$ and a $(2m+1)nddl \times 1$ vector Y:

$$\mathbf{W}\mathbf{T}(t)Y = \mathbf{T}(t)\mathbf{N_W}Y \tag{7}$$

with $\mathbf{N_W} = \mathrm{diag}(\mathbf{W},\mathbf{W},\dots)_{\substack{(2m+1)nddl \\ \times(2m+1)nddl}}$.

Eq. (6) becomes

$$\mathbf{T}(t)\mathbf{N_M}\boldsymbol{\nabla}^2 Z + \mathbf{T}(t)\mathbf{N_D}\boldsymbol{\nabla} Z + \mathbf{T}(t)\mathbf{N_K}Z = \mathbf{T}(t)b$$

$$\mathbf{T}(t)(\mathbf{N_M}\boldsymbol{\nabla}^2 + \mathbf{N_D}\boldsymbol{\nabla} + \mathbf{N_K})Z = \mathbf{T}(t)b \tag{8}$$

Time dependency may be suppressed and a frequency algebraic equation linking Fourier coefficient may be obtained using a Galerkin method which is a projection of the equation on trigonometric functions. Indeed these trigonometric functions define a scalar product:

$$\langle f,g \rangle = \frac{1}{T}\int_0^T f(t)g(t)\,\mathrm{d}t \tag{9}$$

Thus we may write

$$\frac{1}{T}\int_0^T {}^T\mathbf{T}(t)\mathbf{T}(t)\,\mathrm{d}t = \frac{1}{2}\begin{bmatrix} 2\mathbf{I} & & & \mathbf{0} \\ & \mathbf{I} & & \\ & & \mathbf{I} & \\ \mathbf{0} & & & \ddots \end{bmatrix} = \mathbf{L}_{\substack{(2m+1)nddl \\ \times(2m+1)nddl}} \tag{10}$$

Applying this scalar product on Eq. (8) leads to

$$\frac{1}{T}\int_0^T {}^T\mathbf{T}\mathbf{T}(\mathbf{N_M}\boldsymbol{\nabla}^2 + \mathbf{N_D}\boldsymbol{\nabla} + \mathbf{N_K})Z\,\mathrm{d}t = \frac{1}{T}\int_0^T {}^T\mathbf{T}\mathbf{T}b\,\mathrm{d}t$$

$$\mathbf{L}(\mathbf{N_M}\boldsymbol{\nabla}^2 + \mathbf{N_D}\boldsymbol{\nabla} + \mathbf{N_K})Z = \mathbf{L}b \tag{11}$$

$\mathbf{L}$ is a diagonal matrix so Eq. (11) may be simplified into a $(2m+1)*nddl$ equation system:

$$\mathbf{A}Z = b \quad \text{with } \mathbf{A} = \mathbf{N_M}\boldsymbol{\nabla}^2 + \mathbf{N_D}\boldsymbol{\nabla} + \mathbf{N_K} \tag{12}$$

$\mathbf{A}$ may be expressed in a simpler manner

$$\mathbf{A} = \begin{bmatrix} \mathbf{K} & & & & & & \\ & \mathbf{K}-\left(\dfrac{\Omega}{v}\right)^2\mathbf{M} & -\dfrac{\Omega}{v}\mathbf{D} & & & & \\ & \dfrac{\Omega}{v}\mathbf{D} & \mathbf{K}-\left(\dfrac{\Omega}{v}\right)^2\mathbf{M} & & & & \\ & & & \ddots & & & \\ & & & & \mathbf{K}-\left(\dfrac{k}{v}\Omega\right)^2\mathbf{M} & -\dfrac{k}{v}\Omega\mathbf{D} & \\ & & & & \dfrac{k}{v}\Omega\mathbf{D} & \mathbf{K}-\left(\dfrac{k}{v}\Omega\right)^2\mathbf{M} & \\ & & & & & & \ddots \end{bmatrix} \tag{13}$$

This system is equivalent of finding zeros of a function $H : \mathbb{R}^{(2m+1)\times nddl} \to \mathbb{R}^{(2*m+1)\times nddl}$:

$$H(Z) = \mathbf{A}(\Omega)Z - b(Z,\Omega) \tag{14}$$

We note that b is dependent on Z and Ω because b corresponds to the Fourier coefficients of $F(X,\dot{X},\Omega,t)$. In the case where no analytical expression may be written between b and Z, an evaluation of the approximate temporal terms $X(t)$ and $\dot{X}(t)$ is carried out from an initial value $Z = {}^T[B_0 A_1 B_1 \dots A_m B_m]$:

$$Z \xrightarrow{\text{FFT}} X(t) = B_0 + \sum_{k=1}^m \left(A_k \sin\left(\frac{k}{v}\Omega t\right) + B_k \cos\left(\frac{k}{v}\Omega t\right) \right) \tag{15}$$

It also allows to evaluate temporarily the nonlinear term $F_{NL}(X,\dot{X},\Omega,t)$ and then to deduce Fourier coefficients by a *FFT* procedure

$$F_{\mathrm{NL}}(X,\dot{X},\Omega,t) \xrightarrow{\text{FFT}} b_{\mathrm{NL}}(Z,\Omega) = {}^T[C_0^{\mathrm{NL}}\ S_1^{\mathrm{NL}}\ C_1^{\mathrm{NL}}\ \dots\ S_m^{\mathrm{NL}}\ C_m^{\mathrm{NL}}] \tag{16}$$

2.2. Condensation

An additional step can reduce the number of equations to solve. It consists in expressing Fourier coefficients of dofs on which no nonlinearity is applied (called linear dofs) functions of Fourier coefficients of remaining dofs (called nonlinear dofs) and of Fourier coefficients of linear and nonlinear forces:

First, dofs are reorganized into p linear dofs and q nonlinear dofs using a boolean transition matrix $\mathbf{P}$:

$$X = \mathbf{P}\begin{bmatrix} X_p \\ X_q \end{bmatrix} = [\mathbf{P}_p \ \mathbf{P}_q]\begin{bmatrix} X_p \\ X_q \end{bmatrix} \tag{17}$$

where $\mathbf{P}_p$ is a $nddl \times p$ matrix containing the first p columns of $\mathbf{P}$, $\mathbf{P}_p$ contains the last q columns of $\mathbf{P}$.

Using the same decomposition for Fourier coefficients, $Z_p = [B_{0p} \ A_{1p} \ B_{1p} \ \ldots \ A_{mp} \ B_{mp}]^{\mathrm{T}}$ (idem for Z_q), the following result is obtained:

$$Z = [\mathbf{N}_{\mathbf{P}_p} \ \mathbf{N}_{\mathbf{P}_q}]\begin{bmatrix} Z_p \\ Z_q \end{bmatrix} \tag{18}$$

Note that $\mathbf{N}_{\mathbf{P}_p}$ and $\mathbf{N}_{\mathbf{P}_q}$ are respectively $(2m+1)nddl \times (2m+1)p$ and $(2m+1)nddl \times (2m+1)q$ matrices. $\mathbf{N}_{\mathbf{P}}$ and $\mathbf{P}$ are both boolean matrices too and ${}^{T}\mathbf{N}_{\mathbf{P}}\mathbf{N}_{\mathbf{P}} = \mathbf{I}$.

Furthermore, the same property is observed for the vector b so that Eq. (12) becomes

$$\underbrace{\begin{bmatrix} {}^{T}\mathbf{N}_{\mathbf{P}_p}\mathbf{A}\mathbf{N}_{\mathbf{P}_p} \ {}^{T}\mathbf{N}_{\mathbf{P}_p}\mathbf{A}\mathbf{N}_{\mathbf{P}_q} \\ {}^{T}\mathbf{N}_{\mathbf{P}_q}\mathbf{A}\mathbf{N}_{\mathbf{P}_p} \ {}^{T}\mathbf{N}_{\mathbf{P}_q}\mathbf{A}\mathbf{N}_{\mathbf{P}_q} \end{bmatrix}}\begin{bmatrix} Z_p \\ Z_q \end{bmatrix} = \begin{bmatrix} b_p \\ b_q \end{bmatrix} \tag{19}$$

$$\begin{bmatrix} \mathbf{F}_{pp} & \mathbf{F}_{pq} \\ \mathbf{F}_{qp} & \mathbf{F}_{qq} \end{bmatrix}$$

Z_p may be eliminated, and then the system is equivalent of finding zeros of a function $H_q : \mathbb{R}^{(2m+1)\times q} \to \mathbb{R}^{(2*m+1)\times q}$:

$$H_q(Z_q) = (\mathbf{F}_{qq} - \mathbf{F}_{qp}\mathbf{F}_{pp}^{-1}\mathbf{F}_{pq})Z_q - (b_q - \mathbf{F}_{qp}\mathbf{F}_{pp}^{-1}b_p) \tag{20}$$

If the decomposition is chosen so that no force (linear or nonlinear) is applied on the p linear dofs, then $b_p = 0$ and:

$$H_q(Z_q) = \mathbf{A}_q(\Omega)Z_q - b_q(Z_q, \Omega) \tag{21}$$

with $\mathbf{A}_q(\Omega) = \mathbf{F}_{qq} - \mathbf{F}_{qp}\mathbf{F}_{pp}^{-1}\mathbf{F}_{pq}$.

Finally Fourier coefficients of p linear dofs Z_p may be obtained using the relation

$$Z_p = \mathbf{F}_{pp}^{-1}(b_p - \mathbf{F}_{pq}Z_q) \tag{22}$$

2.3. Prediction and correction

For a given frequency Ω, the problem is equivalent to solving a function $\tilde{H}(\tilde{x},\Omega) : \mathbb{R}^k \times \mathbb{R} \to \mathbb{R}^k$ with $\tilde{H} = H$, $\tilde{x} = Z$ and $k = nddl$ or with $\tilde{H} = H_q$, $\tilde{x} = Z_q$ and $k = q$ in the condensation case.

When a simulation has to be done on a frequency band $[\Omega_1; \Omega_2]$, continuation methods have to be applied to follow the solutions and plot the curve $\tilde{H}(\tilde{x},\Omega) = 0$. These methods are based on one or more previous points $[(\tilde{x}_n, \Omega_n), (\tilde{x}_{n-1}, \Omega_{n-1}), \ldots]$ of the response curve from which a prediction $(\tilde{x}_{n+1}^{(0)}, \Omega_{n+1}^{(0)})$ of the next point $(\tilde{x}_{n+1}, \Omega_{n+1})$ is made. Obviously, the closer to the next solution the prediction is, the smaller the number of iterations will be. In order to be able to compute solutions when turning points are present, a curvilinear abscissa s is used. Then, a correction procedure is applied on the prediction, in order to reach after some iterations the next point $(\tilde{x}_{n+1}, \Omega_{n+1})$. In this study no branch points are considered.

Then the main prediction and correction methods are presented. The notation $y = {}^{T}[\tilde{x}\Omega] \in \mathbb{R}^{k+1}$ will be used in the following.

Prediction methods: Three prediction methods are presented and illustrated in Fig. 1(a) for $y \in \mathbb{R}^2$. A given increment Δs of the curvilinear abscissa is used to calculate the prediction.

Secant method: the prediction is on the line defined by the two previous points $\tilde{y}_n, \tilde{y}_{n-1}$:

$$y_{n+1}^0 = y_n + \Delta s \frac{y_n - y_{n-1}}{\|y_n - y_{n-1}\|} \tag{23}$$

Tangent method: the prediction is on the tangent to the curve at the previous point y_n. The direction is given by a unit vector $\vec{t}$ tangent to the jacobian matrix $\mathbf{J}_y\tilde{H}(y_n)$ at the point y_n so

$$y_{n+1}^{(0)} = y_n + \Delta s\,\vec{t} \tag{24}$$

with $\mathbf{J}_y\tilde{H}(y_n)\vec{t} = 0$ and $\det\begin{pmatrix} \mathbf{J}_y\tilde{H}(y_n) \\ {}^{T}\vec{t} \end{pmatrix} > 0$.
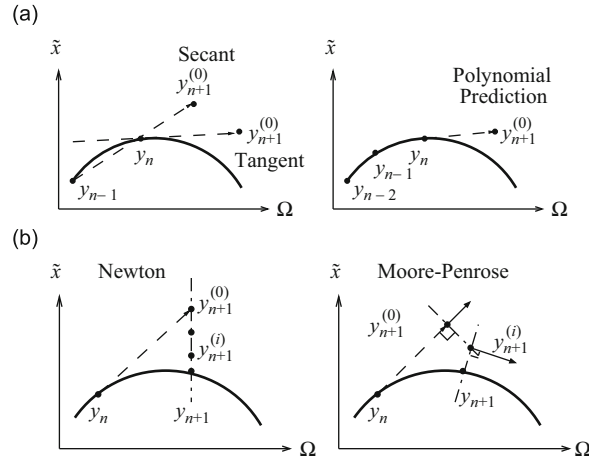
Fig. 1. Prediction and correction methods.

Lagrange polynomial method: the prediction is on a polynomial P of degree d which reaches the $d+1$ previous points $[(y_n,s_n),\ldots,(y_{n-d},s_{n-d})]$. An analytical description of this polynomial may be easily written by using Lagrange polynomials:

$$P(s) = \sum_{i=n-d}^{n} \left(y_i \prod_{\substack{j=n-d \\ j \neq i}}^{n} \frac{s-s_j}{s_i-s_j} \right) \tag{25}$$

The prediction is then calculated by evaluating P for the abscissa $s_n+\Delta s$:

$$y_{n+1}^{(0)} = P(s_n+\Delta s) \tag{26}$$

Correction methods: We consider a prediction $y_{n+1}^{(0)} \in \mathbb{R}^{k+1}$ of the next solution so the system is not square because the function $\tilde{H}$ offers only k equations. One component of y (often the parameter Ω) has to be fixed or one more equation is added to the system. The correction methods are presented in Fig. 1(b). Correction on $\tilde{x}$ and Ω are noted $\Delta\tilde{x}$ and $\Delta\Omega$.

Newton method: one component Ω_{n+1} is fixed to the prediction value $\Omega_{n+1}^{(0)}$. Then the system is a square system which can be solved by using a Newton–Raphson procedure. For the i th iteration, the corrected point is

$$y_{n+1}^{(i)} = \begin{bmatrix} \tilde{x}_{n+1}^{(i)} + \Delta\tilde{x} \\ \Omega_{n+1} \end{bmatrix} \quad \text{with } \Delta\tilde{x} = -\mathbf{J}_{\tilde{x}}\tilde{H}(\tilde{x}_{n+1}^{(i)},\Omega_{n+1})\tilde{H}(\tilde{x}_{n+1}^{(i)},\Omega_{n+1}) \tag{27}$$

Moore–Penrose method: the vector defined by two consecutive points $y_{n+1}^{(i+1)}$ and $y_{n+1}^{(i)}$ is orthogonal to the kernel of the jacobian matrix $\mathbf{J}_y\tilde{H}(y_{n+1}^{(i)})$ of $\tilde{H}$ to the point $y_{n+1}^{(i)}$. The Moore–Penrose matrix inverse defined as $\mathbf{W}^+ = {}^T\mathbf{W}(\mathbf{W}^T\mathbf{W})^{-1}$ for matrix $\mathbf{W}$ is used. The following expression is obtained:

$$y_{n+1}^{(i)} = y_{n+1}^{(0)} + \begin{bmatrix} \Delta\tilde{x} \\ \Delta\Omega \end{bmatrix} \quad \text{with } \begin{bmatrix} \Delta\tilde{x} \\ \Delta\Omega \end{bmatrix} = -\mathbf{J}_y^+\tilde{H}(y_{n+1}^{(i)})\tilde{H}(y_{n+1}^{(i)}) \tag{28}$$

Adaptive step: If a step Δs used to make a prediction is too large, the number of iterations will be too time-consuming or the solution may not be found. Furthermore, a too large step may lead to difficulties in the vicinity of turning points. So an adaptive step is often appropriate and different methods are available. A widespread tool is to consider the previous number of iterations and to reduce the step when solver takes more iterations than an optimal chosen value. A larger step is chosen when the number of iterations is lower than a minimal value too. Many numerical criteria may be developed to limit the step variation.

2.4. Proposed criterion

For a given excitation frequency of the system, no theoretical tool exists to determine which harmonics are really predominant. Furthermore the number of necessary harmonics can strongly vary for the studied frequency interval. Some numerical tools have been developed, in particular the work of Laxalde [23] who developed a method based on the degree of approximation of the nonlinearity. This criterion does not take into account the global system behavior and may not be adapted when linear forces are predominant in comparison to nonlinear forces. Consequently the criterion presented in this section focuses on approximate system strain energy and on its evolution for different numbers of harmonics in the response.

Approximate strain energy: First, for a response developed in a Fourier series, the system strain energy U may be expressed as

$$U = \frac{1}{2}\,^T X(t)\mathbf{K}X(t) = \frac{1}{2}\,^T Z\,^T \mathbf{T}(t)\mathbf{T}(t)\mathbf{N_K}Z \tag{29}$$

We may suppress the time dependency by calculating the mean value on one period:

$$\langle U \rangle = \frac{1}{2}\,^T Z\mathbf{LN_K}Z \tag{30}$$

Approximate strain energy for a condensation: When a reduction on q nonlinear dofs is used, the strain energy expression must be adapted in order to be computed only from Fourier coefficients Z_q of the q nonlinear dofs and to avoid the time consuming step which consists in calculating linear Fourier coefficients Z_p.

First some properties must be noted.

For a condensation procedure, the boolean transition matrix $\mathbf{P}$ is used. System matrices $\mathbf{M}$ (respectively $\mathbf{D}$ and $\mathbf{K}$) may be rearranged to correspond to the dofs division $[X_p \ X_q]^T$ by using the following conversion $\tilde{\mathbf{M}} = \,^T \mathbf{PMP}$ (respectively $\tilde{\mathbf{D}}$ and $\tilde{\mathbf{K}}$). Similarly to $\mathbf{F}$ in Eq. (19), $\tilde{\mathbf{M}}$ may be divided in four blocks:

$$\tilde{\mathbf{M}}_{kl} = \,^T \mathbf{P}_k \mathbf{M} \mathbf{P}_l \quad \text{with } (k,l) \in \{p,q\} \tag{31}$$

Furthermore, for a $r \times s$ matrix $\mathbf{W}$ and a $s \times t$ matrix $\mathbf{V}$, $\mathbf{N_W N_V} = \mathbf{N_{WV}}$ and $\,^T \mathbf{N_W} = \mathbf{N}_{^T \mathbf{W}}$.

Then, if the matrix $\text{diag}(\mathbf{0}_{k \times k}, \boldsymbol{\nabla}_1, \ldots, \boldsymbol{\nabla}_m)$ with identity matrix as $\mathbf{I}_{k \times k}$ is named $\boldsymbol{\nabla}_k$, the following formula may be obtained:

$$\boldsymbol{\nabla} \mathbf{N}_{\mathbf{P}_k} = \mathbf{N}_{\mathbf{P}_k} \boldsymbol{\nabla}_k \quad \text{with } k \in \{p,q\} \tag{32}$$

Finally, the matrix $\mathbf{L}_k$ is a $(2m+1)k \times (2m+1)k$ matrix with identity matrix as $\mathbf{I}_{k \times k}$ and $k \in \{p,q\}$.

For the computation of criterion in the reduction case, Eq. (30) becomes

$$\langle U \rangle = \frac{1}{2}\,^T Z\mathbf{LN_K}Z$$

$$\langle U \rangle = \frac{1}{2}[\,^T Z_p \ ^T Z_q]\begin{bmatrix} ^T \mathbf{N}_{\mathbf{P}_p} \\ ^T \mathbf{N}_{\mathbf{P}_q} \end{bmatrix}\mathbf{LN_K}[\mathbf{N}_{\mathbf{P}_p} \ \mathbf{N}_{\mathbf{P}_q}]\begin{bmatrix} Z_p \\ Z_q \end{bmatrix}$$

$$\langle U \rangle = \frac{1}{2}[\,^T Z_p \ ^T Z_q]\begin{bmatrix} \mathbf{L}_p & \mathbf{0} \\ \mathbf{0} & \mathbf{L}_q \end{bmatrix}\begin{bmatrix} \mathbf{N}_{\mathbf{P}_p\mathbf{KP}_p} & \mathbf{N}_{\mathbf{P}_p\mathbf{KP}_q} \\ \mathbf{N}_{\mathbf{P}_q\mathbf{KP}_p} & \mathbf{N}_{\mathbf{P}_q\mathbf{KP}_q} \end{bmatrix}\begin{bmatrix} Z_p \\ Z_q \end{bmatrix}$$

$$\langle U \rangle = \frac{1}{2}(^T Z_p \mathbf{L}_p \mathbf{N}_{\tilde{\mathbf{K}}_{pp}} Z_p + \,^T Z_p \mathbf{L}_p \mathbf{N}_{\tilde{\mathbf{K}}_{pq}} Z_q + \,^T Z_q \mathbf{L}_q \mathbf{N}_{\tilde{\mathbf{K}}_{qp}} Z_p + \,^T Z_q \mathbf{L}_q \mathbf{N}_{\tilde{\mathbf{K}}_{qq}} Z_q) \tag{33}$$

Then, a more explicit form of matrix $\mathbf{F}$ (Eq. (19)) must be established

$$\mathbf{F}_{kl} = \,^T \mathbf{N}_{\mathbf{P}_k} \mathbf{A} \mathbf{N}_{\mathbf{P}_l} \tag{34}$$

Introducing the expression of matrix $\mathbf{A}$ of Eq. (12) leads to

$$\mathbf{F}_{kl} = \,^T \mathbf{N}_{\mathbf{P}_k}(\mathbf{N_M}\boldsymbol{\nabla}^2 + \mathbf{N_D}\boldsymbol{\nabla} + \mathbf{N_K})\mathbf{N}_{\mathbf{P}_l}$$

$$\mathbf{F}_{kl} = \mathbf{N}_{\tilde{M}_{kl}}\boldsymbol{\nabla}_l^2 + \mathbf{N}_{\tilde{D}_{kl}}\boldsymbol{\nabla}_l + \mathbf{N}_{\tilde{K}_{kl}} \tag{35}$$

with $(k,l) \in \{p,q\}$. For simplicity, linear and nonlinear Fourier coefficients are supposed to be linked in a static case ($\Omega = 0$) so that $\boldsymbol{\nabla}_l = \mathbf{0}_{l \times l}$.

By using this assumption in Eq. (22), Z_p may be expressed as

$$Z_p = \mathbf{N}_{\tilde{K}_{pp}}^{-1}(b_p - \mathbf{N}_{\tilde{K}_{pq}}Z_q) \tag{36}$$

If the decomposition is chosen so that no force (linear or nonlinear) is applied on the p linear dofs, then $b_p = 0$ and

$$Z_p = -\mathbf{N}_{\tilde{K}_{pp}}^{-1} \mathbf{N}_{\tilde{K}_{pq}} Z_q \tag{37}$$

By replacing Eq. (37) into Eq. (33):

$$\langle U \rangle = \frac{1}{2}(^T Z_q\,_{\tilde{K}_{\tilde{p}q}}^T \mathbf{N}\tilde{\mathbf{K}}_{pq}\,^T \mathbf{N}_{\tilde{\mathbf{K}}_{pp}^{-1}}\mathbf{L}_p\mathbf{N}_{\tilde{\mathbf{K}}_{pp}}\mathbf{N}_{\tilde{\mathbf{K}}_{pp}^{-1}}\mathbf{N}_{\tilde{\mathbf{K}}_{pq}}Z_q + \,^T Z_q\,^T\mathbf{N}_{\tilde{\mathbf{K}}_{pq}}\,^T\mathbf{N}_{\tilde{\mathbf{K}}_{pp}^{-1}}\mathbf{L}_p\mathbf{N}_{\tilde{\mathbf{K}}_{pq}}Z_q + \,^T Z_q\mathbf{L}_q\mathbf{N}_{\tilde{\mathbf{K}}_{qp}}\mathbf{N}_{\tilde{\mathbf{K}}_{pp}^{-1}}\mathbf{N}_{\tilde{\mathbf{K}}_{pq}}Z_q + \,^T Z_q\mathbf{L}_q\mathbf{N}_{\tilde{\mathbf{K}}_{qq}}Z_q)$$

$$\langle U \rangle = \frac{1}{2}\,^T Z_q\mathbf{L}_q\mathbf{N}_{\tilde{\mathbf{K}}_{qq} - ^T\tilde{\mathbf{K}}_{qp}\tilde{\mathbf{K}}_{pp}^{-1}\tilde{\mathbf{K}}_{pq}}Z_q \tag{38}$$

This equation is very similar to Eq. (30) obtained for the nonreduced case. Matrix $\tilde{\mathbf{K}}_{qq} - \,^T\tilde{\mathbf{K}}_{qp}\tilde{\mathbf{K}}_{pp}^{-1}\tilde{\mathbf{K}}_{pq}$ acts as reduced stiffness matrix on the q nonlinear dofs.
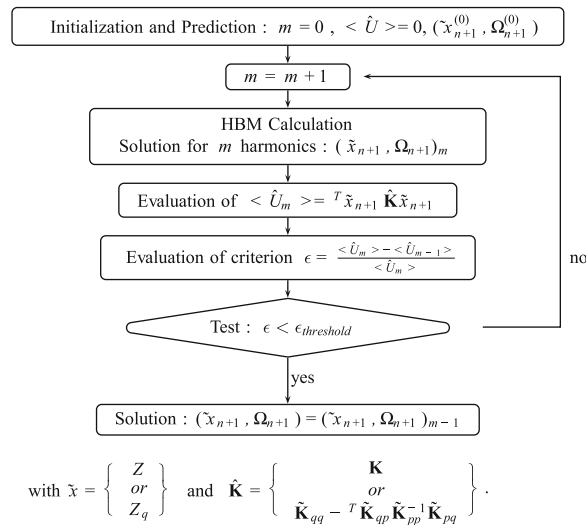
Fig. 2. Algorithm for criterion ε.

Criterion ε: The criterion ε developed in this section is computed for a given frequency and the first resolution is performed for one harmonic. Then the relative difference between two consecutive values of strain energy is evaluated. The first value is obtained for m harmonics and the second for $m+1$ harmonics. The increase is stopped when ε becomes less than a threshold chosen by user. Algorithm is detailed in Fig. 2.

As matrices **L** and $\mathbf{L}_q$ are diagonal constant block matrices and as algorithm starts for one harmonic, studying strain energy saturation is equivalent to studying saturation of an approximate quantity:

$$\langle \hat{U} \rangle = {}^T Z \mathbf{N_K} Z \quad \text{without condensation}$$

$$\langle \hat{U} \rangle = {}^T Z_q \mathbf{N}_{\tilde{\mathbf{K}}_{qq} - {}^T\tilde{\mathbf{K}}_{qp}\tilde{\mathbf{K}}_{pp}^{-1}\tilde{\mathbf{K}}_{pq}} Z_q \quad \text{with condensation} \tag{39}$$

Finally, when the convergence rate of the strain energy turns out to be nonsmooth, the method may stop before saturation. For example, for dry friction systems, only odd harmonics appear. However, as shown later, this drawback may be avoided removing all even harmonics in the calculation. For other cases, for example when the 1st and 5th harmonics responds, this drawback constitutes a limitation of the method.

3. Application case

3.1. Two beam system and joint model

A two cantilever beam system linked by a bolted joint is considered for simulations in order to illustrate the selection process of harmonics and is shown in Fig. 3(a). Beams are made of aluminum 7075 Al and the section is rectangular ($5.1\,\text{cm} \times 2.5\,\text{cm}$). The two beams have different lengths (34.7 and 84.7 cm) in order to avoid a symmetric behavior.

Beams are modelled with Abaqus software with two dimensional B21 beam elements which use a Timoshenko formulation. 10 (respectively 25) elements are used for the 34.7 cm (respectively 84.7 cm) beam. Due to axial forces, geometric nonlinearities may appear in this clamped-clamped beam system for high level of excitation and may be simultaneously present with joint nonlinearity. However this model is focused on localized nonlinearities and study has been limited to joint nonlinearities. For further details on geometric nonlinearities, the reader can refer to Sze et al. [24] who applied HBM on a nonlinear beam.

Bolted joint is represented with a 3.5 cm long element described by a mass elementary matrix of a B21 beam element and a nonlinear stiffness matrix considered as an external force. These external forces are the two moments M_1 and M_2 and the two forces T_1 and T_2. A Rayleigh damping is calculated by using mass and stiffness matrices of a monolithic beam so that damping has a value of 0.1 percent for frequencies of 0.24 and 1.14 kHz. These two frequencies correspond to the second and fifth modes. The value of 0.1 percent is representative of real structures and remains sufficiently low to keep a significative nonlinearity impact. Indeed, a material damping increase leads to reduce vibration amplitudes and consequently higher order harmonics amplitudes so adaptive harmonic balance method will retain a smaller number of harmonics.

Nonlinear stiffness model of bolted joint presented in Fig. 3(b) is largely inspired by a previous work of Song [14] and uses a model called adjusted LuGre beam element (ALBE) by analogy with Song's work. Frictional slip and slapping
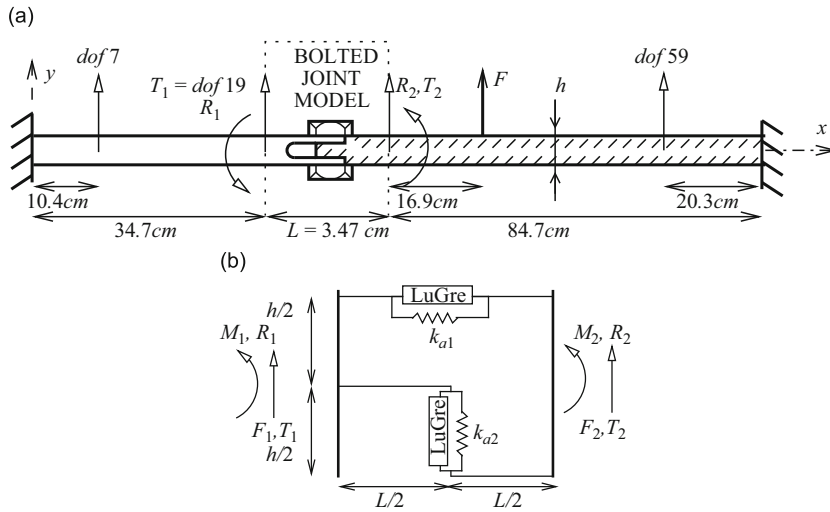
Fig. 3. Application case (a) two beam system and (b) bolted joint model.

constitutes the two main nonlinear phenomena involved in the joint interface [10]. However, for the sake of simplicity, slapping which can lead to higher order harmonics has not been considered in this study. Frictional slip is here considered with a nonlinear model integrating a LuGre model leading to odd harmonics. As discussed in Section 2.4, even harmonics have to be removed in the HBM calculation so that smooth convergence rate of strain energy is observed on only odd harmonics. The basic idea is to replace stiffnesses of a linear beam element by a parallel combination of a LuGre model and a residual stiffness $k_{a,i}, i \in 1,2$ characteristic of a bolted joint [11]. The element has two rotational dofs $R1$ and $R2$ and two translational dofs $T1$ and $T2$. h and L are respectively section height and element length.

Spring elongations Δ_1 and Δ_2 have to be considered to express relation between nonlinear force $F_{NL,ALBE}$ and element dofs:

$$\Delta_1 = \frac{L}{2}(R_1 + R_2) + (T1 + T2) \quad \text{and} \quad \Delta_2 = \frac{h}{2}(R_1 - R_2) \tag{40}$$

Consequently each LuGre force $f_{LuGre,i}, i \in 1,2$ depends on Δ_i elongation but also on internal variable value ζ_i and its derivative $\dot{\zeta}_i$. It may be written as

$$f_{LuGre,i}(\Delta_i, \dot{\Delta}_i, \zeta_i, \dot{\zeta}_i) = \sigma_{0i}\Delta_i + \sigma_{1i}\dot{\zeta}_i + \alpha_{2i}\dot{\Delta}_i \tag{41}$$

$$\dot{\zeta}_i = \dot{\Delta}_i - \frac{\sigma_{0i}}{\alpha_{0i} + \alpha_{1i}e^{-(\dot{\Delta}_i/v_{0i})^2}}|\dot{\Delta}_i|\zeta_i \tag{42}$$

The combination of one LuGre model and one spring provides a force which takes the following form:

$$f_i(\Delta_i, \dot{\Delta}_i, \zeta_i, \dot{\zeta}_i) = f_{LuGre,i}(\Delta_i, \dot{\Delta}_i, \zeta_i, \dot{\zeta}_i) + k_{a,i}\Delta_i \tag{43}$$

Stiffness decrease during microslip regimes may be represented by using a coefficient $\gamma_i \in [0;1]$ which links the residual stiffness $k_{a,i}$, the LuGre model stiffness parameter σ_{0i} and the equivalent linear element stiffness k_i. The relative equations are $\sigma_{0i} = (1-\gamma_i)k_i$ and $k_{a,i} = \gamma_i k_i$.

Forces F_1, F_2 and resulting moments M_1, M_2 may be expressed as

$$\begin{bmatrix} F1 \\ M1 \\ F2 \\ M2 \end{bmatrix} = \begin{bmatrix} f_1(\Delta_1, \dot{\Delta}_1, \zeta_1, \dot{\zeta}_1) \\ \frac{L}{2}f_1(\Delta_1, \dot{\Delta}_1, \zeta_1, \dot{\zeta}_1) + \frac{h}{2}f_2(\Delta_2, \dot{\Delta}_2, \zeta_2, \dot{\zeta}_2) \\ -f_1(\Delta_1, \dot{\Delta}_1, \zeta_1, \dot{\zeta}_1) \\ \frac{L}{2}f_1(\Delta_1, \dot{\Delta}_1, \zeta_1, \dot{\zeta}_1) - \frac{h}{2}f_2(\Delta_2, \dot{\Delta}_2, \zeta_2, \dot{\zeta}_2) \end{bmatrix} \tag{44}$$

Thus from Eq. (40) forces $F_{NL,ALBE}$ may be written as a function of ALBE dofs:

$$F_{NL,ALBE}\left(\begin{bmatrix} T_1 \\ R_1 \\ T_2 \\ R_2 \end{bmatrix}, \begin{bmatrix} \dot{T}_1 \\ \dot{R}_1 \\ \dot{T}_2 \\ \dot{R}_2 \end{bmatrix}, \begin{bmatrix} \zeta_1 \\ \zeta_2 \end{bmatrix}, \begin{bmatrix} \dot{\zeta}_1 \\ \dot{\zeta}_2 \end{bmatrix}\right) = \begin{bmatrix} F1 \\ M1 \\ F2 \\ M2 \end{bmatrix} \tag{45}$$

The two equivalent linear element stiffnesses k_i are obtained by the following relations:

$$k_1 = 12\frac{EI}{L^3} = 1.43 \times 10^6 \, \text{N/mm} \quad \text{and} \quad k_2 = 4\frac{EI}{Lh^2} = 8.92 \times 10^5 \, \text{N/mm} \tag{46}$$

Other parameters are deduced by analogy with Shiryayev's work [25], namely $\gamma_1 = \gamma_2 = 0.1078$, $\alpha_{01} = \alpha_{02} = 81.9 \, \text{N}$, $\sigma_{11} = \sigma_{12} = \alpha_{11} = \alpha_{12} = \alpha_{21} = \alpha_{22} = 0$. Finally $\sigma_{01} = 1.27 \times 10^6 \, \text{N/mm}$, $\sigma_{02} = 7.96 \times 10^5 \, \text{N/mm}$, $k_{a,1} = 1.55 \times 10^5 \, \text{N/mm}$, $k_{a,2} = 9.62 \times 10^4 \, \text{N/mm}$.

Then the system is excited with a harmonic excitation F_L of 42 N with a pulsation Ω. Load is applied on the longest beam on translational dof 31. By using formulation introduced in Eq. (1), one may write the governing equation of motion to which two equations have to be added. These additional equations describe LuGre model internal variables ζ_1, ζ_2 evolution

$$\mathbf{M}\ddot{X} + \mathbf{D}\dot{X} + \mathbf{K}X = F_L(\Omega,t) - F_{\text{NL,ALBE}}\left(\begin{bmatrix} X \\ \dot{X} \end{bmatrix}, \begin{bmatrix} \zeta_1 \\ \zeta_2 \end{bmatrix}, \begin{bmatrix} \dot{\zeta}_1 \\ \dot{\zeta}_2 \end{bmatrix}, \Omega, t\right) \tag{47}$$

$$\dot{\zeta}_i = \dot{\Delta}_i - \frac{\sigma_{0i}}{\alpha_{0i} + \alpha_{1i}e^{-(\dot{\Delta}_i/v_{0i})^2}} |\dot{\Delta}_i|\zeta_i \quad \text{for } i \in \{1,2\} \tag{48}$$

3.2. Adaptation of HBM formulation to LuGre model

In the studied case, two equations are added to the equation of motion and integrate nonlinear terms. Thus an adaptation of HBM formulation becomes necessary. To do so, the two internal variables ζ_1 and ζ_2 are developed as a Fourier series in the same way as X. By inserting the truncature $\zeta_i(t) = \mathbf{T}(t)Z_{\zeta_i}$ into Eq. (48), the same Galerkin method is applied on the resulting equation and one obtains

$$0 = \dot{\zeta}_i - \left(\dot{\Delta}_i - \frac{\sigma_{0i}}{\alpha_{0i} + \alpha_{1i}e^{-(\dot{\Delta}_i/v_{0i})^2}} |\dot{\Delta}_i|\zeta_i\right)$$

$$0 = \mathbf{T}(t)\nabla Z_{\zeta_i} - \mathbf{T}(t)b_{\zeta_i}(Z, Z_{\zeta_i}, \Omega)$$

$$0 = \mathbf{N}_{\mathbf{I}_{1 \times 1}}\nabla Z_{\zeta_i} - b_{\zeta_i}(Z, Z_{\zeta_i}, \Omega) \quad \text{with } i \in \{1,2\} \tag{49}$$

where $b_{\zeta_i}(Z, Z_{\zeta_i}, \Omega)$ are Fourier coefficients of the nonlinear term.

Consequently the problem is equivalent to finding zeros of a function $HH(Z, Z_\zeta)$ depending on Fourier coefficients of X and $\zeta = [\zeta_1 \; \zeta_2]$. These coefficients are named Z and $Z_\zeta = [Z_{\zeta_1} \; Z_{\zeta_2}]$. HH is a function from $\mathbb{R}^{(2m+1)\times(nddl+2)}$ to $\mathbb{R}^{(2*m+1)\times(nddl+2)}$.

$$HH(Z, Z_\zeta) = \left\{ \begin{array}{l} H(Z, Z_\zeta) = \mathbf{A}(\Omega)Z - b(Z, Z_\zeta, \Omega) \\ C(Z, Z_\zeta) = \mathbf{N}_{\mathbf{I}_{2 \times 2}}\nabla Z_\zeta - b_\zeta(Z, Z_\zeta, \Omega) \end{array} \right\} \tag{50}$$

In case of condensation, we may define similarly a function $HH_q(Z_q, Z_\zeta)$ from $\mathbb{R}^{(2m+1)\times(q+2)}$ to $\mathbb{R}^{(2*m+1)\times(q+2)}$:

$$HH_q(Z_q, Z_\zeta) = \left\{ \begin{array}{l} H_q(Z_q, Z_\zeta) = \mathbf{A}_q(\Omega)Z_q - b_q(Z_q, Z_\zeta, \Omega) \\ C(Z_q, Z_\zeta) = \mathbf{N}_{\mathbf{I}_{2 \times 2}}\nabla Z_\zeta - b_{q,\zeta}(Z_q, Z_\zeta, \Omega) \end{array} \right\} \tag{51}$$

Finally, calculation of approximate strain energy $\langle \hat{U} \rangle$ stay the same as Eqs. (33) and (38) because only Fourier coefficients of physical dofs are used to quantify strain energy.

3.3. Results

In the following, shown results have been calculated on the frequency band, 0–2.3 kHz with a curvilinear abscissa and an adaptive step to better describe resonance peaks. The Moore–Penrose method is used for correction at each iteration and prediction is made with Lagrange polynomials of degree 2.

3.3.1. Nonlinear effects on dynamic responses

The maximal amplitude of vibration obtained for the linear case and for the two different nonlinear cases (one harmonic case and adaptive case) are presented in Fig. 4(a–c) for the three dofs of the system. The 1 harmonic case refers here to the classical HBM with one harmonic and does not refer to an adaptive algorithm. The first dof 7 is located on the left beam, the second is a translational dof 19 corresponding to the R 1 dof of the ALBE model, and the third one is the dof 59 on the right beam. Fig. 3(a) details the dof position on the system. The threshold value for the relative variation of the approximate strain energy has been fixed to 3 percent and excitation force has an amplitude of 42 N. The linear case shows seven modes on the studied frequency band. First nonlinearity effects are significant on the one harmonic response and result in two phenomena: a reduction of resonance peak amplitudes which reflects the damping from the joint and a modal softening which reflects the joint stiffness decrease. Thus some modes have important frequency shifts and even significant distortions, notably the second, fifth and sixth modes. Frequency shifts and vibration amplitude reductions have the same order of magnitude for all the considered dofs. Differences are observed between the 1 harmonic curve and the adaptive
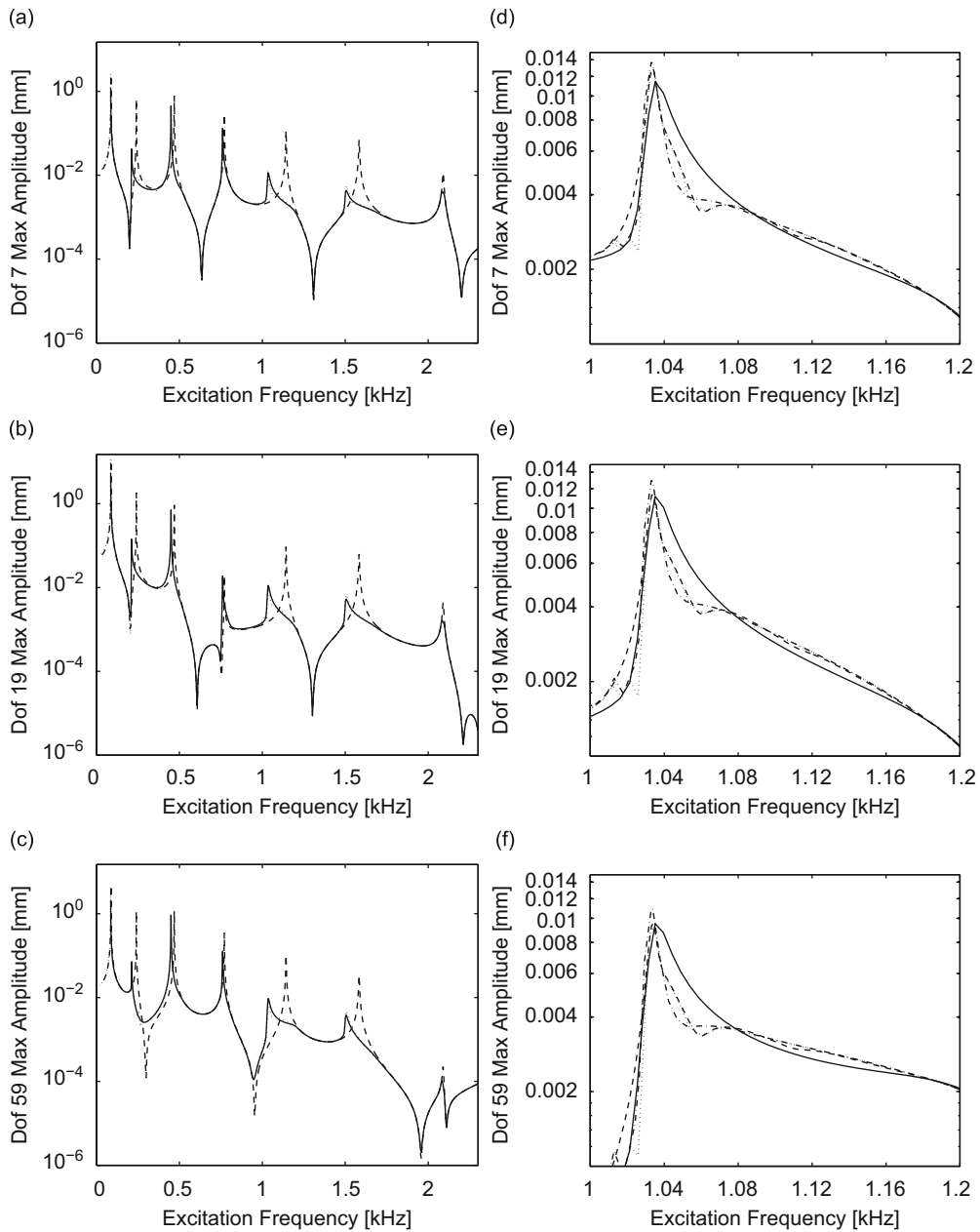
Fig. 4. Maximal amplitude of vibration for dofs 7(a, d), 19(d, e), 59(c, f) and for different linear and nonlinear cases: (a–c) over all the frequency band; – – (linear, HBM 1 harm.); — (nonlinear, HBM 1 harm.); … (nonlinear, adaptive HBM) (d–f) zoom on 1.1 kHz resonance; — (nonlinear, HBM 1 harm.); –.– (nonlinear, HBM 3 harm.); … (nonlinear, adaptive HBM); –.– (nonlinear, HBM 11 harm.)

algorithm near resonances especially near the fifth and sixth modes where the shape of peaks differs. Far from resonance peaks, adaptive algorithm give the same results as the 1 harmonic calculation.

Figs. 4(d–f) present a zoom on the 1.1 kHz resonance peak. Three nonlinear cases corresponding to a calculation with 1, 3 and 11 harmonics are compared with the adaptive HBM curve. Near the resonance, the adaptive HBM remains close to the response with 11 harmonics. However, Fig. 5, which plots the number of harmonics over the whole frequency band, shows that the number of harmonics reaches only 7 harmonics at most, revealing satisfying convergence of the method. The number of used harmonics may vary from 1 to 11 for resonance peaks but only 1 harmonic is necessary elsewhere. It shows that nonlinear phenomena are more pronounced on resonances. The maximum number of harmonics has been fixed to 15 in this case.

Contribution of each harmonic (1st, 3rd and 5th harmonic) is shown in Fig. 6(a–c) by plotting the Fourier coefficient modulus of the 1st, 3rd and 5th harmonics of the vibration response ($\|A_k\,B_k\|$ for harmonic k and for one dof into Eq. (2)) near the 1.1 kHz resonance peak. Analyses are still performed on the three dofs 7, 19, and 59. For the all three dofs, the 1st
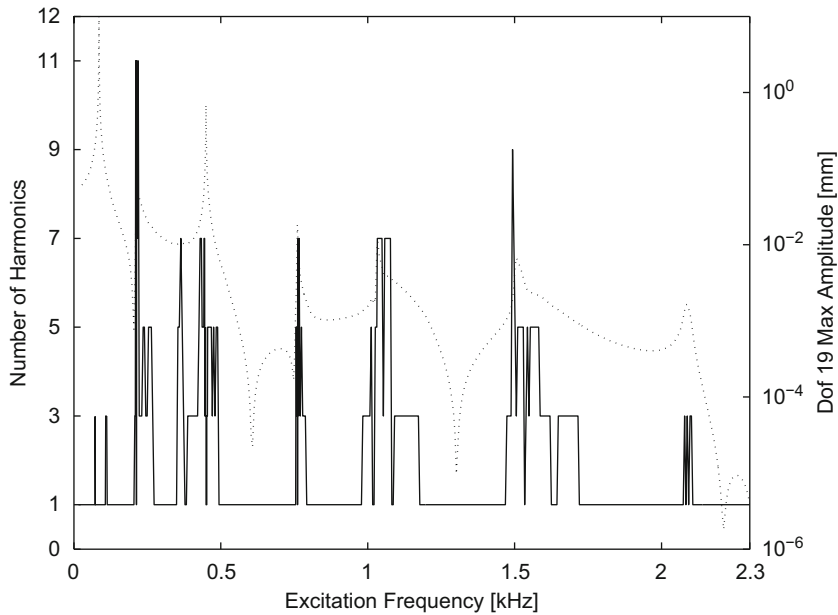
Fig. 5. Evolution of the number of harmonics: — number of harmonics; … maximal amplitude of vibration for dof 19.

harmonic contribution remains larger than the 3rd and 5th harmonic contributions. However, analysis of the ratios 3rd/1st (Fig. 6(d–f)) and 5th/1st (Fig. 6(g–i)) shows that importance of third and fifth harmonics increases near resonances and may represent up to 10 percent for the third harmonic and up to 2 percent for the fifth harmonic. This observation may be linked with the work of Ouyang et al. [22] who found emergence of third and fifth superharmonics which represented about respectively 2 and 0.7 percent of the first harmonic. It may also be noted that third and fifth harmonics are less predominant for dof 7 than for dofs 19 and 59.

A similar analysis on the approximate strain energy may be carried out by considering the contribution of the order k as being the term $\frac{1}{2}{}^T Z_k \mathbf{K} Z_k$. Z_k refers here to the contribution of the order k to the Fourier coefficient vector Z of the vibration response. Results are plotted in Fig. 7(a). Ratios 3rd/1st and 5th/1st are shown in Fig. 7(b, c). The same tendency that for maximal amplitude of vibration with a peak near resonance frequencies is observed. Moreover, ratios have the same order of magnitude with a maximum value of 12.5 percent for the third harmonic and of 2 percent for the fifth harmonic, revealing that approximate strain energy behaves like a global indicator of each dof behavior.

3.3.2. Approximate strain energy saturation

Approximate strain energy $\langle \hat{U} \rangle$ is presented over all the frequency band for three cases on Fig. 8(a). The first case shows the shape of $\langle \hat{U} \rangle$ for a linear case and a peak is observed for each resonance frequency. The other two cases correspond to nonlinear calculations with one harmonic and with an adaptive number of harmonics. Nonlinear effects decrease vibration amplitude of the system so that peaks on approximate strain energy are attenuated. As observed on the maximal amplitude of vibration curves, peaks are shifted to the left. Moreover, differences between linear and nonlinear cases are predominant near resonance frequencies and adaptive algorithm curve differs from one harmonic curve showing an increase in the required number of harmonics. A zoom near the 1.1 kHz peak is made on Fig. 8(b) in order to show convergence of the approximate strain energy quantity. Results are presented for 1, 3 and 11 harmonics and for the adaptive case. Saturation is observed and adaptive case stays close to 11 harmonic curve even if no more than 9 harmonics are used. Finally, it has to be noted that strain energy saturation is directly tested on odd harmonics due to the presence of dry friction in the model and considered harmonics have a monotonous decrease of their amplitude. It constitutes a limitation of the method which cannot deal with nonconsecutive predominant harmonics (for example system with 1, 3 and 11 predominant harmonics).

3.3.3. Influence of force excitation

First simulations were carried out with an excitation amplitude of 42 N. Influence of excitation force amplitude on nonlinear effects is now investigated by varying amplitude with the values 6, 12, 24, 42, 66N. The maximal amplitude of vibration is presented for the three considered dofs in Fig. 9. Zooms for the dof 19 are done for the first three peaks in Fig. 9(a), for the fifth peak in Fig. 9(b) and for the seventh peak in Fig. 9(c). Responses are computed by using the adaptive algorithm. First, we note that an increase in excitation amplitude results in larger vibration amplitudes, and this
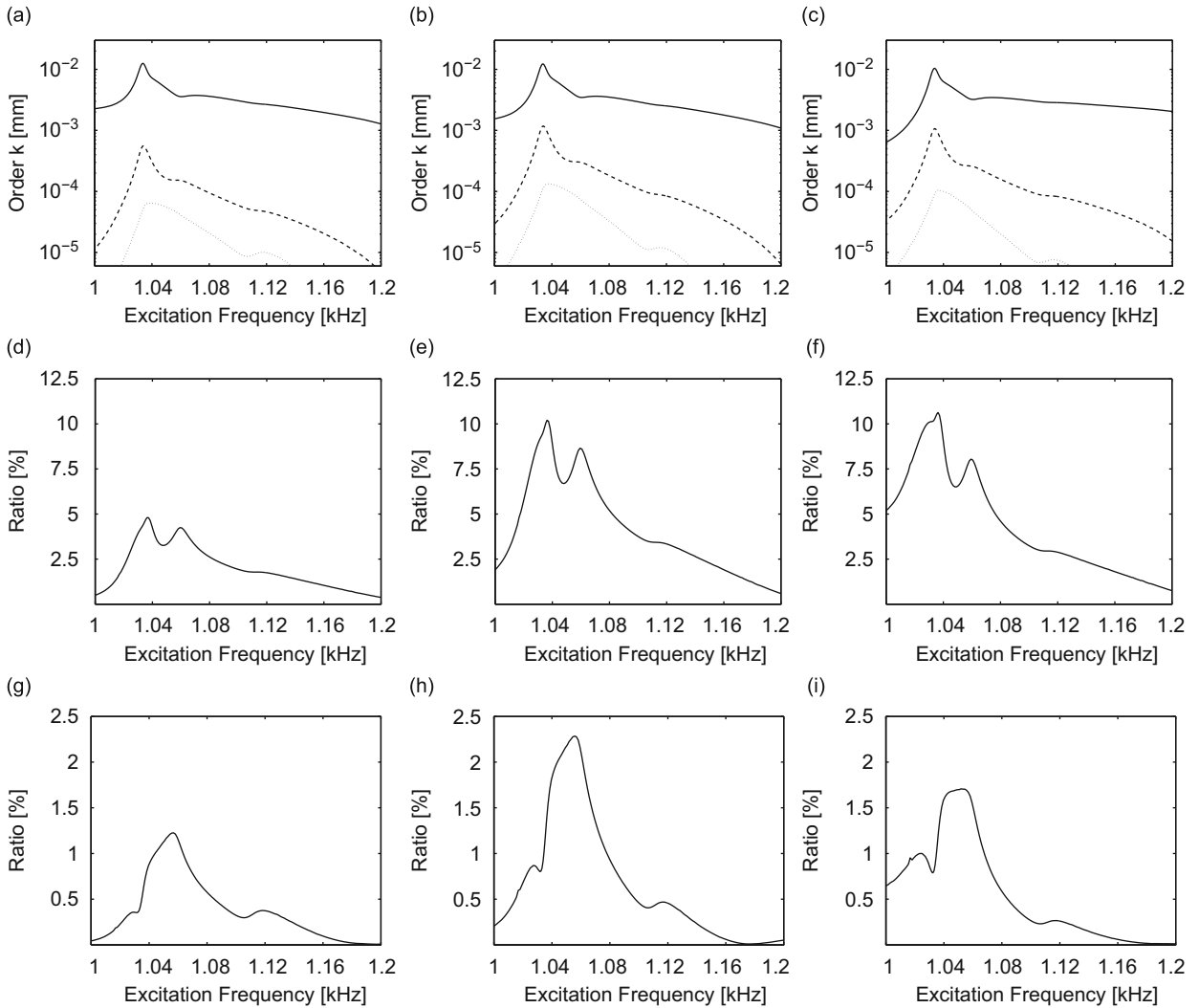
Fig. 6. Contribution of 1st, 3rd and 5th harmonics on maximal amplitude of vibration and associated ratios for dofs 7(a, d, g), 19(b, e, h), 59(c,f,i): (a–c) Fourier coefficient modulus of the: — 1st harmonic; – – 3rd harmonic; … 5th harmonic; (d–f) ratio 3rd/1st; (g–i) ratio 5th/1st.
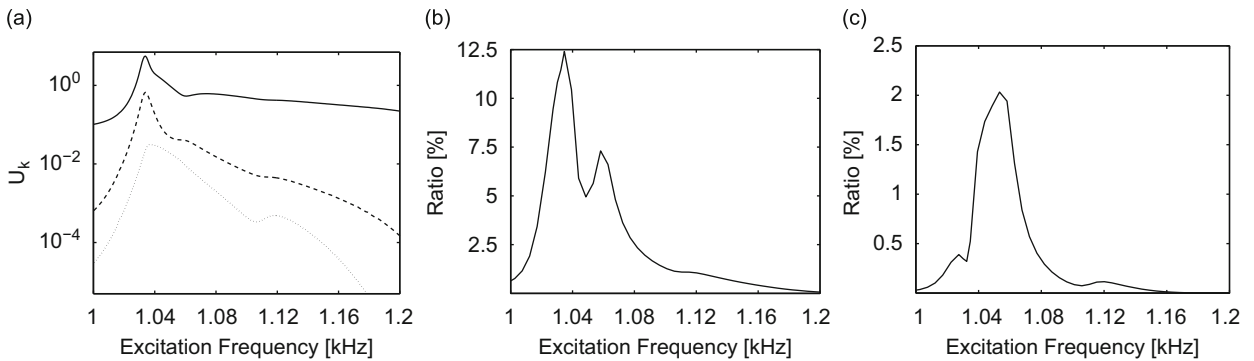

Fig. 7. Contribution of 1st, 3rd and 5th harmonics on approximate strain energy and associated ratios: (a) contribution of the: — 1st harmonic; – – 3rd harmonic; … 5th harmonic; (b) ratio 3rd/1st; (c) ratio 5th/1st.

for all the three dofs. Then, the main notable nonlinear effect is an increase in modal softening for larger excitation amplitude, as shown by left shifts of resonance peaks. It clearly shows a relationship between modal softening and vibration amplitudes and this dependence is nonlinear as previously noticed by Ungar [4]. For larger amplitudes, this
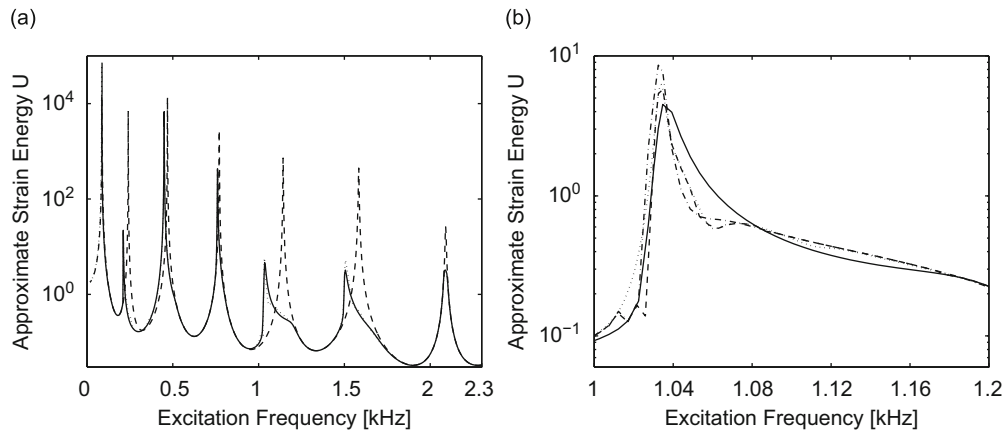
Fig. 8. Approximate strain energy for different linear and nonlinear cases: (a) over all the frequency band; – – (linear, HBM 1 harm.); — (nonlinear, HBM 1 harm.); ... (nonlinear, adaptive HBM) (b) zoom on 1.1 kHz resonance; — (nonlinear, HBM 1 harm.); –.– (nonlinear, HBM 3 harm.); ... (nonlinear, adaptive HBM); –.– (nonlinear, HBM 11 harm.)

modal softening becomes less remarkable revealing the beginning of macro-slip and so the stabilization of the contact stiffness (Fig. 10).

In order to compare the five nonlinear cases, frequency response functions (FRFs) are computed by dividing the maximal amplitude of vibration by the excitation force amplitude for each frequency value. Results, which are very similar for the three considered dofs, are presented in the particular case of the dof 19 in Fig. 11 for all the frequency band (a), for the first three peaks (b), for the fifth peak (c) and for the seventh peak (d). First we note that modal softening is still observed on resonance peaks and FRF maximal value decreases when excitation amplitude increases, reaching a minimal value between the 24 and 42 N cases before a new increase for larger excitation amplitudes, except for the 2.2 kHz peak where only a decrease is observed. Damping provided by joints is nonlinear and amplitude dependent and this may explain this behavior. Ouyang et al. [22] observed the same phenomenon on the relation between energy dissipation and excitation amplitude for a torsional joint and notices that, as excitation amplitude becomes larger, micro-slip increases.

Excitation amplitude has an influence on nonlinear effects and consequently on the number of harmonics used by the adaptive algorithm. Fig. 12(a–e) presents the number of obtained harmonics for the five different excitation values. A zoom on the 1.1 kHz peak is done. For the lowest amplitude value, the adaptive HBM only requires one harmonic whereas for the highest amplitude it uses nine harmonics. This increase is progressive and the frequency interval for which more than one harmonic are needed widens. Left shifts of resonances are also noticeable because the frequency for which the number of harmonics is maximum decreases as excitation amplitude becomes higher.

3.3.4. Influence of threshold value

Three threshold values of 1, 3, 5 percent have been tested for the adaptive algorithm. Fig. 13(a–c) shows the evolution of the number of harmonics for the two peaks near 1.1 kHz and 1.5 kHz and for these three threshold values. Unsurprisingly, an increase of the selected number of harmonics is observed when the threshold value decreases because more harmonics are needed to reach this precision. Threshold value still remains a value to be determined by user.

3.3.5. Analysis of general and reduced criteria

An expression of approximate strain energy has been established in Eq. (38) when a condensation procedure is used in order to avoid the calculation of linear Fourier coefficients for each step of the adaptive algorithm. This expression is based on an assumption that linear and nonlinear Fourier coefficients are linked in a static case allowing to obtain an approximate strain energy described only with the reduced stiffness matrix and not with mass and damping matrices. A calculation with this reduced criteria has been carried out and the evolution of the approximate strain energy for the two condensation and general cases are overlaid in Fig. 14(a). The two quantities clearly differ for frequencies higher than that of the first resonance, invalidating the assumption used for the calculation of the strain energy. However Fig. 14(b), which plots the evolution of the number of obtained harmonics when the reduced criterion is used, shows that the result of the adaptive algorithm is very close to the result for the general case presented in Fig. 5. This may be explained by the fact that the used criterion computes a relative quantity and observes strain energy saturation by evaluating a relative difference between two consecutive values. The use of this criterion may represent an alternative for an adaptive HBM calculation.
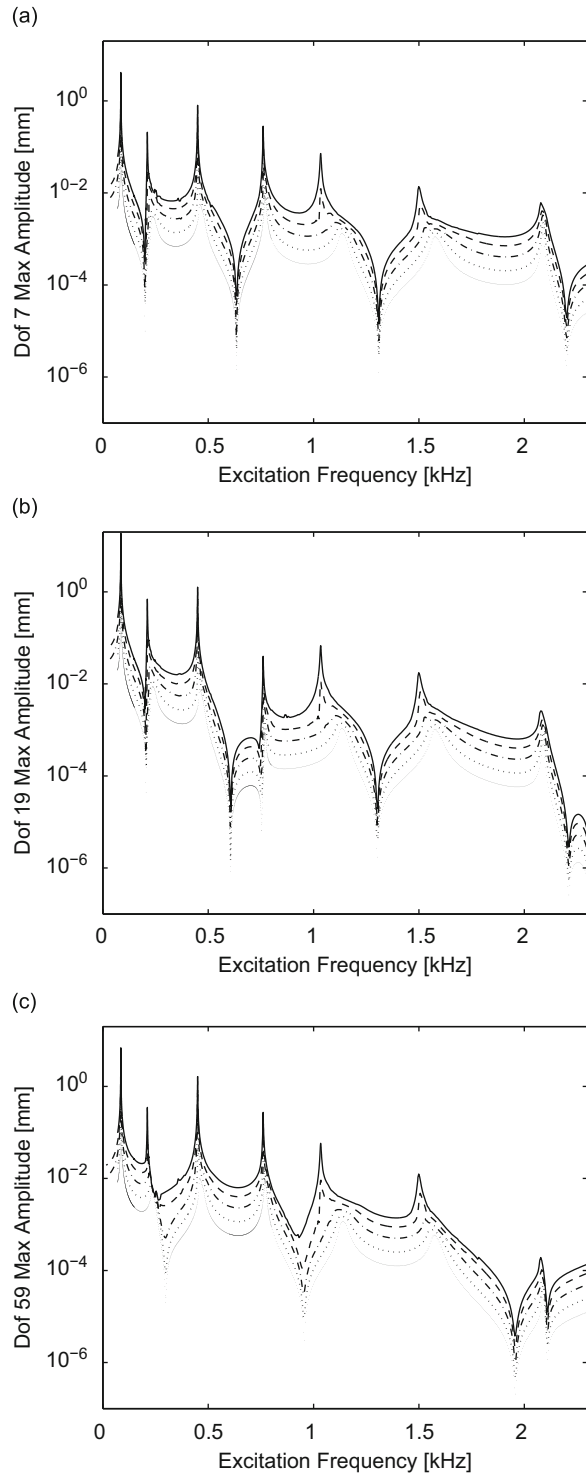
(a)

(b)

(c)

Fig. 9. Influence of excitation force amplitude on maximal amplitude of vibration for dofs 7(a), 19(b), 59(c): … 6 N; - - - 12 N; –.– 24 N; – – 42 N; — 66 N.

4. Conclusion

This article develops a new adaptive harmonic balance method which selects the number of harmonics at each frequency value for a mechanical system integrating localized nonlinearities. A two beam system linked by a bolted joint is
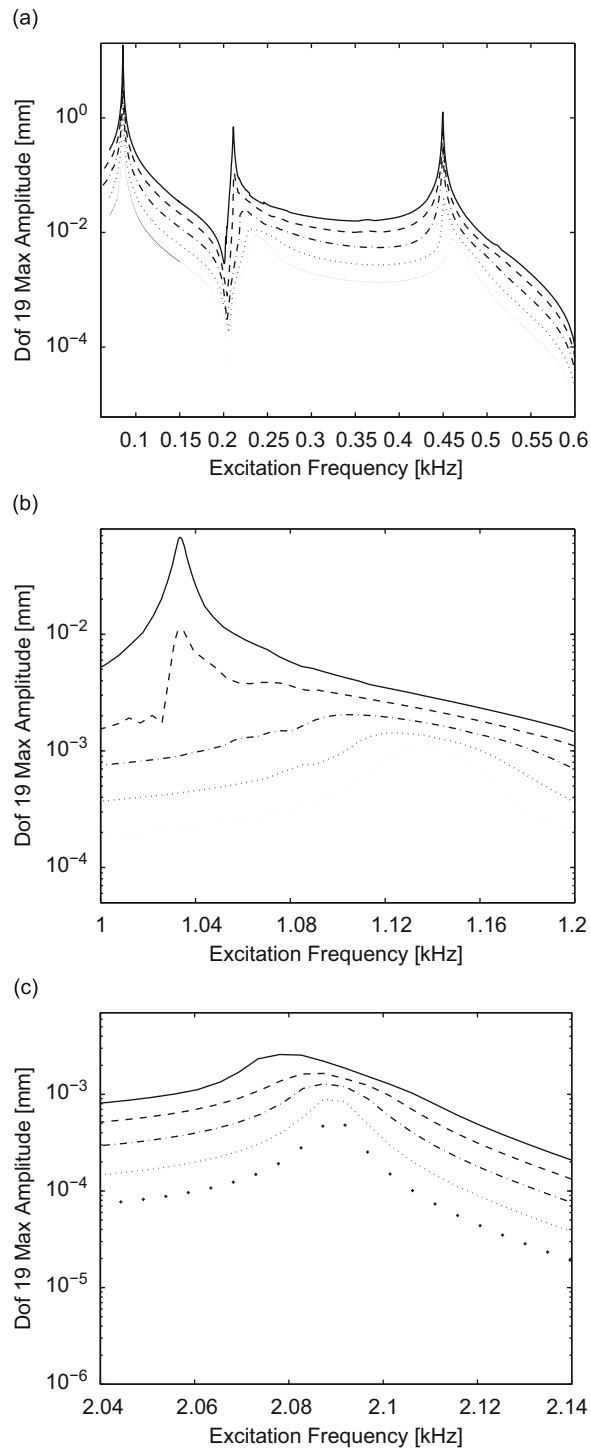
Fig. 10. Influence of excitation force amplitude on maximal amplitude of vibration for dof 19: (a) zoom on 3 first resonances, (b) zoom on 1.1 kHz resonance and (c) zoom on 2 kHz resonance: … (replaced by +++ on (c)) 6 N; - - - 12 N; –.– 24 N; – – 42 N; — 66 N.

chosen for application case. HBM formulation is combined with a reduction on nonlinear dofs of the system and a simulation on a frequency band is carried out by using a prediction method based on Lagrange polynomials and a correction method based on Newton and Moore–Penrose methods. In order to adapt the number of harmonics taken into account at each frequency, an adaptive algorithm has been developed. The method computes an approximate strain energy
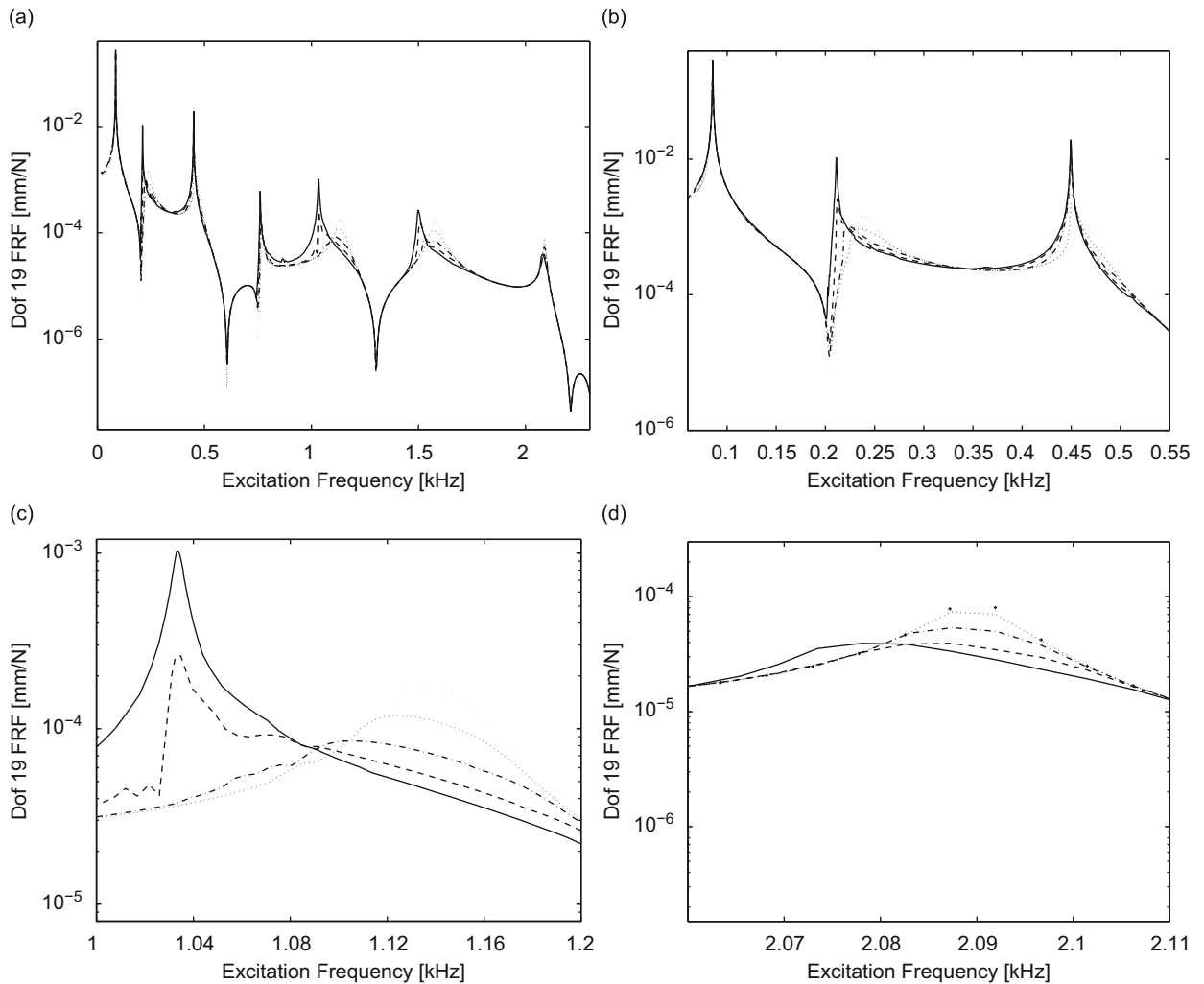
Fig. 11. Influence of excitation force amplitude on frequency response functions for dof 19: (a) over all the frequency band, (b) zoom on three first resonances, (c) zoom on 1.1 kHz resonance, (d) zoom on 2 kHz resonance: … (replaced by +++ on (d)) 6 N; - - - 12 N; –.– 24 N; – – 42 N; — 66 N.

from Fourier coefficients of the response and observes its saturation by evaluating the relative difference between two consecutive cases corresponding to two different number of harmonics. This new criterion, based on Fourier coefficients, does not require time integration and may be easily estimated. In a condensation case, criterion formulation is also expressed. Furthermore geometric nonlinearity due to axial forces in the clamped-clamped beam are not taken into account and nonlinear effects in the joint consider only frictional slip. Slapping is not modelled in this study. Slip in the bolted joint element is represented by a LuGre model which leads to adapt the HBM formulation in order to develop internal variables as Fourier series.

Results show that one harmonic is sufficient to give a satisfactory approximation of the response away from resonances and is necessary to highlight nonlinear effects such as damping of resonance peaks and modal softening. Indeed the dynamic behavior is strongly modified compared with the linear case. Moreover, adaptive HBM shows that, for a given threshold value of the criterion, the number of harmonics may increase on resonances indicating that nonlinear effects are predominant. The evolution of the approximate strain energy shows that a peak is observed near each resonance and saturation of this quantity is noted when the number of harmonics increases. However, calculation is performed only on odd harmonics due to dry friction leading to a smooth convergence rate of the strain energy on tested harmonics. This condition constitutes a limitation of the method which cannot deal with nonconsecutive predominant harmonics (for example system with predominant harmonics 1, 3 and 11). Analysis of each harmonic contribution notices the emergence of third and fifth harmonics both on the response and on approximate strain energy near resonances, showing the global characteristic of the criterion based on approximate strain energy. In order to obtain a wider range of harmonics and to model a more physical bolted system, slapping and geometric nonlinearities could be considered for further work. A
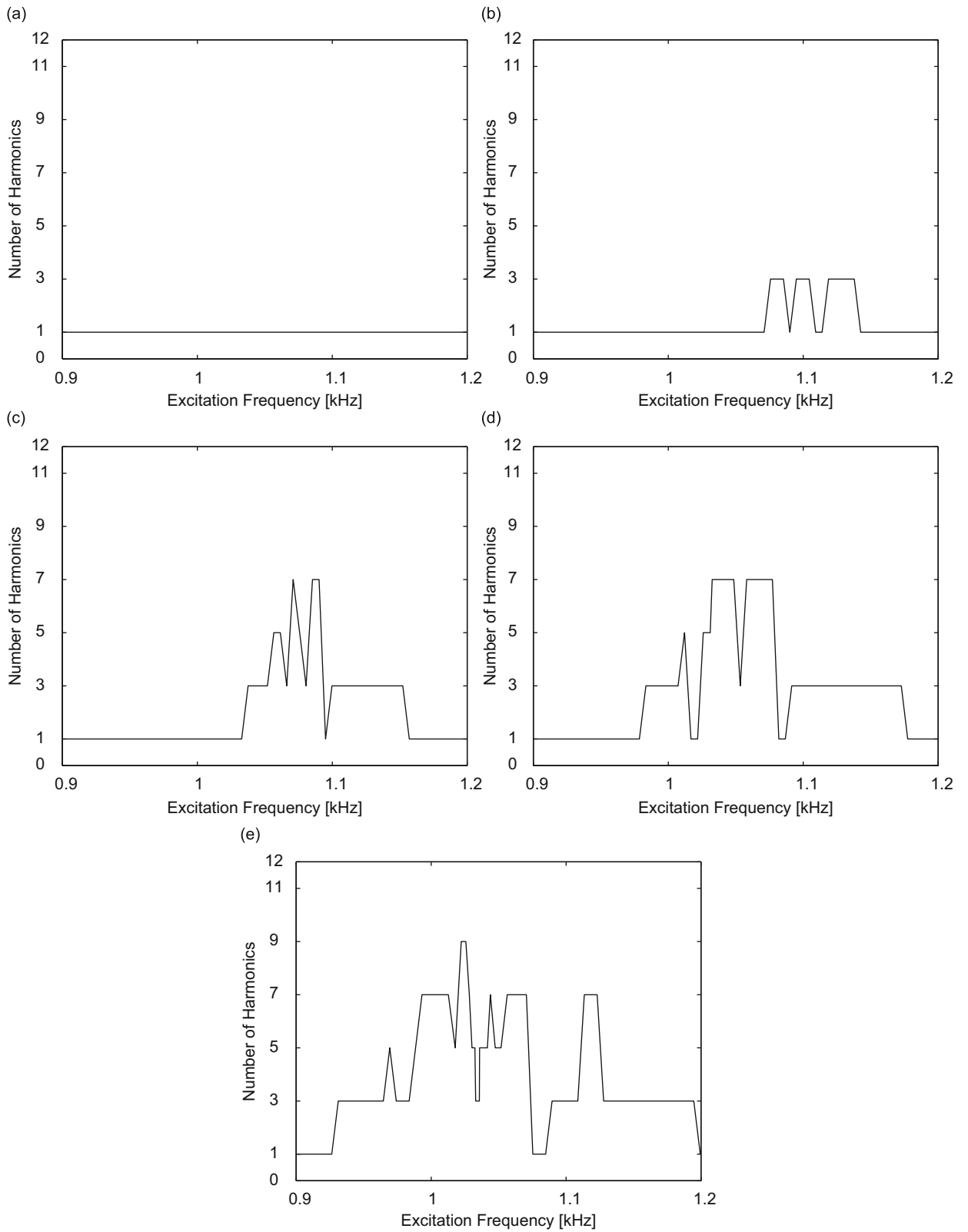
Fig. 12. Influence of excitation force amplitude on the number of harmonics, zoom on the 1.1 kHz resonance: (a) 6 N, (b) 12 N, (c) 24 N, (d) 42 N and (e) 66 N.
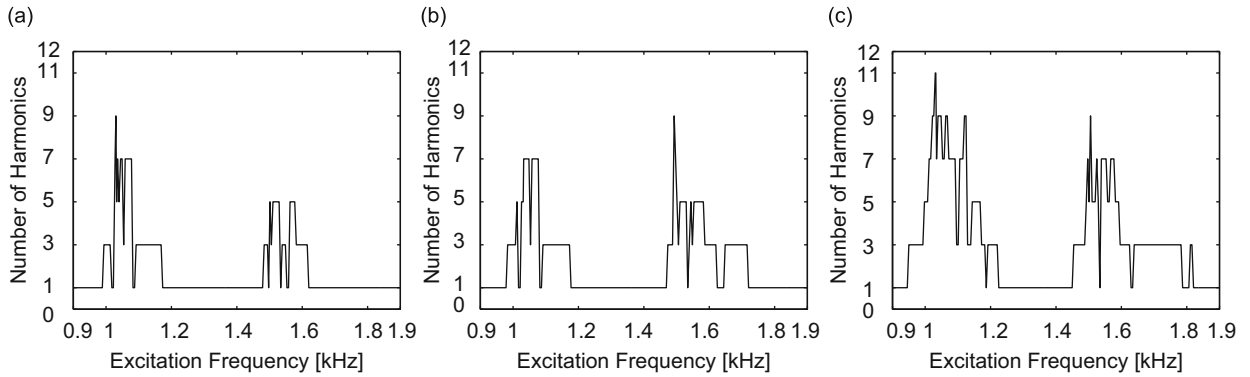
(a)

(b)

(c)

Fig. 13. Influence of threshold value on the number of harmonics, zoom on the 1.1 kHz and the 1.5 kHz resonances: (a) 5 percent, (b) 3 percent and (c) 1 percent.
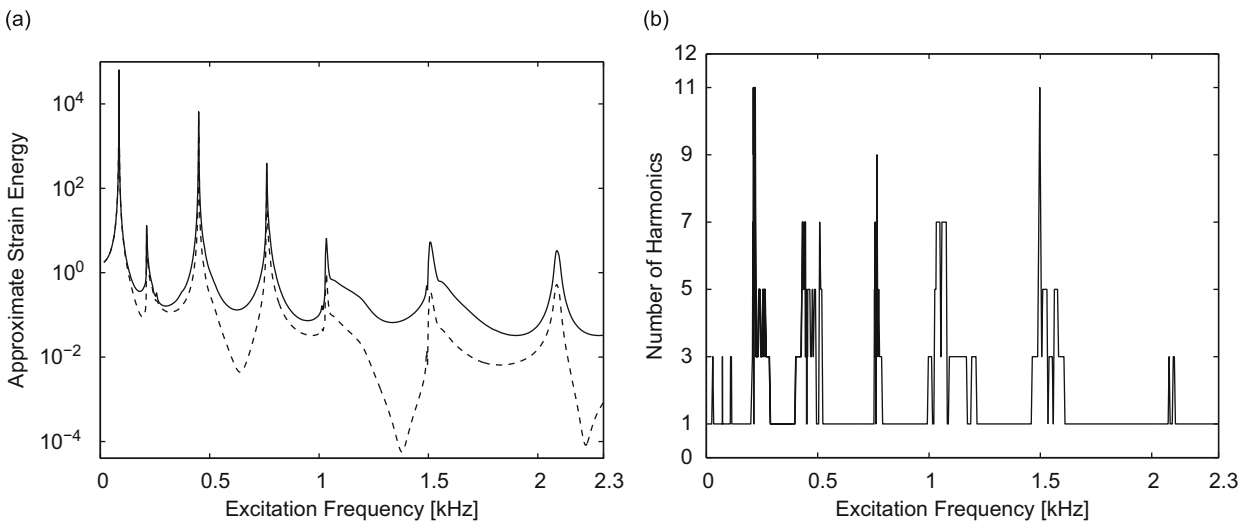
(a)

(b)

Fig. 14. (a) Approximate strain energy: — general expression; – – condensation case expression. (b) Number of harmonics obtained with the condensation case expression.

coherent behavior is noticed when threshold value varies because more harmonics are needed to reach the given precision when threshold value of the adaptive algorithm is decreased.

A parametric study is carried out by varying the excitation force amplitude. Vibration amplitude increases with higher force amplitude because nonlinear effects, notably micro slip in the joint, become more pronounced. Modal softening and damping depends on vibration amplitude and this dependency is nonlinear. Maximum of frequency response functions for each resonance depends nonlinearly on excitation amplitude and may reach a minimum value for an intermediate excitation amplitude. The number of needed harmonics becomes larger for increasing amplitudes underlining the predominance of nonlinear effects.

References

[1] D.J. Segalman, Modelling joint friction in structural dynamics, *Journal of Sound and Vibration* 13 (1) (2005) 430–453.
[2] L. Gaul, R. Nitsche, The role of friction in mechanical joints, *Applied Mechanics Reviews* 54 (2) (2001) 93–106.
[3] C.F. Beards, Damping in structural joints, *The Shock and Vibration Digest* 24 (7) (1992) 3–7.
[4] E.E. Ungar, Status of engineering knowledge concerning damping of built-up structures, *Journal of Sound and Vibration* 26 (1) (1973) 141–154.
[5] R.A. Ibrahim, C.L. Pettit, Uncertainties and dynamic problems of bolted joints and other fasteners, *Journal of Sound and Vibration* 279 (3–5) (2005) 857–936.
[6] H. Ahmadian, J.E. Mottershead, S. James, M.I. Friswell, C.A. Reece, Modelling and updating of large surface-to-surface joints in the awe-mace structure, *Mechanical Systems and Signal Processing* 20 (4) (2006) 868–880.
[7] A.D. Crocombe, R. Wang, G. Richardson, C.I. Underwood, Estimating the energy dissipated in a bolted spacecraft at resonance, *Computers & Structures* 84 (5–6) (2006) 340–350.
[8] R. Wang, A.D. Crocombe, G. Richardson, C.I. Underwood, Energy dissipation in spacecraft structures incorporating bolted joints operating in macroslip, *Journal of Aerospace Engineering* 21 (1) (2008) 19–26.

[9] A. Caignot, P. Ladevèze, D. Néron, V. Le Gallo, L. Gonidou, Virtual testing for the prediction of damping in joints, *ICED 2007 International Conference in Engineering Dynamics*, 2007.

[10] H. Ahmadian, H. Jalali, Generic element formulation for modelling bolted lap joints, *Mechanical Systems and Signal Processing* 21 (5) (2007) 2318–2334.

[11] L. Gaul, J. Lenz, Nonlinear dynamics of structures assembled by bolted joints, *Acta Mechanica* 125 (1–4) (1997) 169–181.

[12] M.J. Oldfield, H. Ouyang, J.E. Mottershead, Simplified models of bolted joints under harmonic loading, *Computers & Structures* 84 (1–2) (2005) 25–33.

[13] H. Ahmadian, H. Jalali, Identification of bolted lap joints parameters in assembled structures, *Mechanical Systems and Signal Processing* 21 (2) (2007) 1041–1050.

[14] Y. Song, C.J. Hartwigsen, D.M. McFarland, A.F. Vakakis, L.A. Bergman, Simulation of dynamics of beam structures with bolted joints using adjusted Iwan beam elements, *Journal of Sound and Vibration* 273 (1–2) (2004) 249–276.

[15] J.D. Miller, D.D. Quinn, A two-sided interface model for dissipation in structural systems with frictional joints, *Journal of Sound and Vibration* 321 (1–2) (2009) 201–219.

[16] L. Heller, E. Foltete, J. Piranda, Experimental identification of nonlinear dynamic properties of built-up structures, *Journal of Sound and Vibration* 327 (1–2) (2009) 183–196.

[17] C. Pierre, A.A. Ferri, E.H. Dowell, Multi-harmonic analysis of dry friction damped systems using an incremental harmonic-balance method, *Journal of Applied Mechanics—Transactions of the ASME* 52 (4) (1985) 958–964.

[18] A.A. Ferri, E.H. Dowell, Frequency-domain solutions to multi-degree-of-freedom dry, friction damped systems, *Journal of Sound and Vibration* 124 (2) (1988) 207–224.

[19] T.M. Cameron, J.H. Griffin, An alternating frequency/time domain method for calculating the steady-state response of nonlinear dynamic systems, *Journal of Applied Mechanics* 56 (1) (1989) 149–154.

[20] N. Coudeyras, J.-J. Sinou, S. Nacivet, A new treatment for predicting the self-excited vibrations of nonlinear systems with frictional interfaces: the constrained harmonic balance method, with application to disc brake squeal, *Journal of Sound and Vibration* 319 (3–5) (2009) 1175–1199.

[21] Y. Ren, T.M. Lim, M.K. Lim, Identification of properties of nonlinear joints using dynamic test data, *Journal of Vibration and Acoustics—Transactions of the ASME* 120 (2) (1998) 324–330.

[22] H. Ouyang, M.J. Oldfield, J.E. Mottershead, Experimental and theoretical studies of a bolted joint excited by a torsional dynamic load, *International Journal of Mechanical Sciences* 48 (12) (2006) 1447–1455.

[23] D. Laxalde, Etude d'amortisseurs non-linéaires appliqués aux roues aubagées et aux systèmes multi-étages. PhD Thesis, Ecole Centrale de Lyon, 2007.

[24] K.Y. Sze, S.H. Chen, J.L. Huang, The incremental harmonic balance method for non linear vibration of axially moving beams, *Journal of Sound and Vibration* 281 (2005) 611–626.

[25] O.V. Shiryayev, S.M. Page, C.L. Pettit, J.C. Slater, Parameter estimation and investigation of a bolted joint model, *Journal of Sound and Vibration* 307 (3–5) (2007) 680–697.